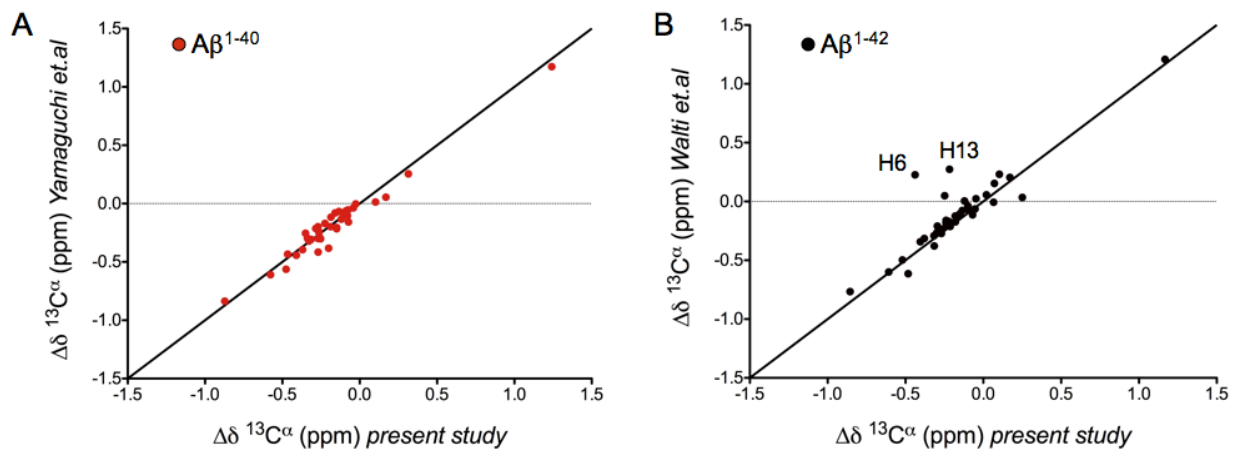


# **Monomeric A $\beta$ <sup>1-40</sup> and A $\beta$ <sup>1-42</sup> Peptides in Solution Adopt Very Similar Ramachandran Map Distributions that Closely Resemble Random Coil**

Julien Roche, Yang Shen, Jung Ho Lee, Jinfa Ying and Ad Bax

Laboratory of Chemical Physics, National Institute of Diabetes and Digestive and Kidney Diseases, National Institutes of Health,  
Bethesda, Maryland, USA

## **SUPPORTING INFORMATION**



**Figure. S1 :** Comparison between the secondary  $^{13}\text{C}^\alpha$  measured in the present study and those reported by Yamaguchi et al.<sup>1</sup> for  $\text{A}\beta^{1-40}$  (A) and by Waelti et al.<sup>2</sup> for  $\text{A}\beta^{1-42}$  (B). The reference random coil values and corrections factors reported by Poulsen et coworkers<sup>3,4</sup> were used to calculate the secondary chemical shifts.

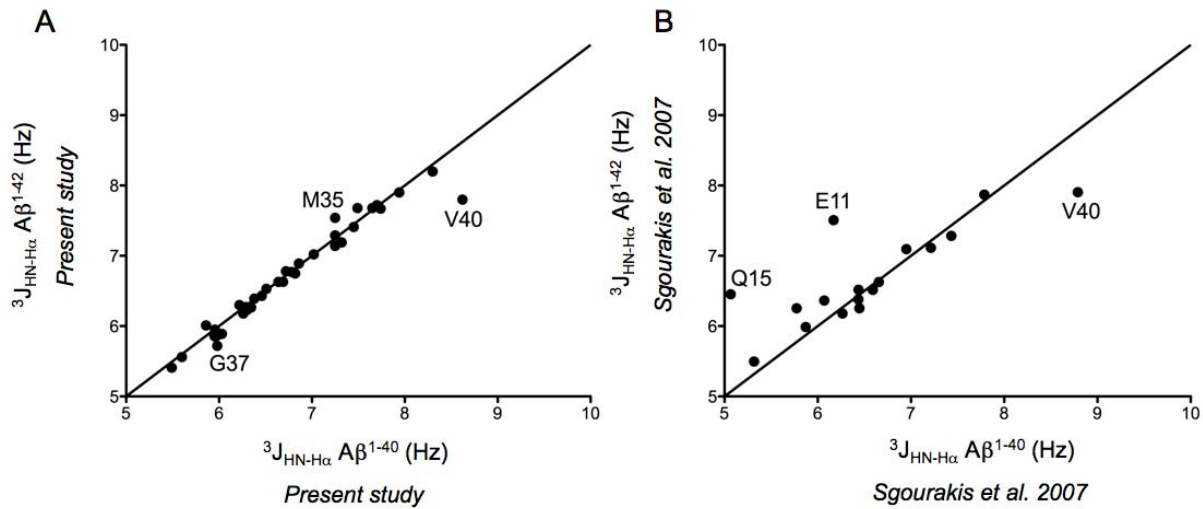


**Figure. S2 :** Comparison of the  $^3J_{\text{HNH}\alpha}$  coupling measured for  $\text{A}\beta^{1-40}$  and  $\text{A}\beta^{1-42}$  in (A) the present study and (B) reported in Sgourakis et al.<sup>5</sup> In each panel the residues presenting the largest  $^3J_{\text{HNH}\alpha}$  coupling differences between  $\text{A}\beta^{1-40}$  and  $\text{A}\beta^{1-42}$  are labeled.

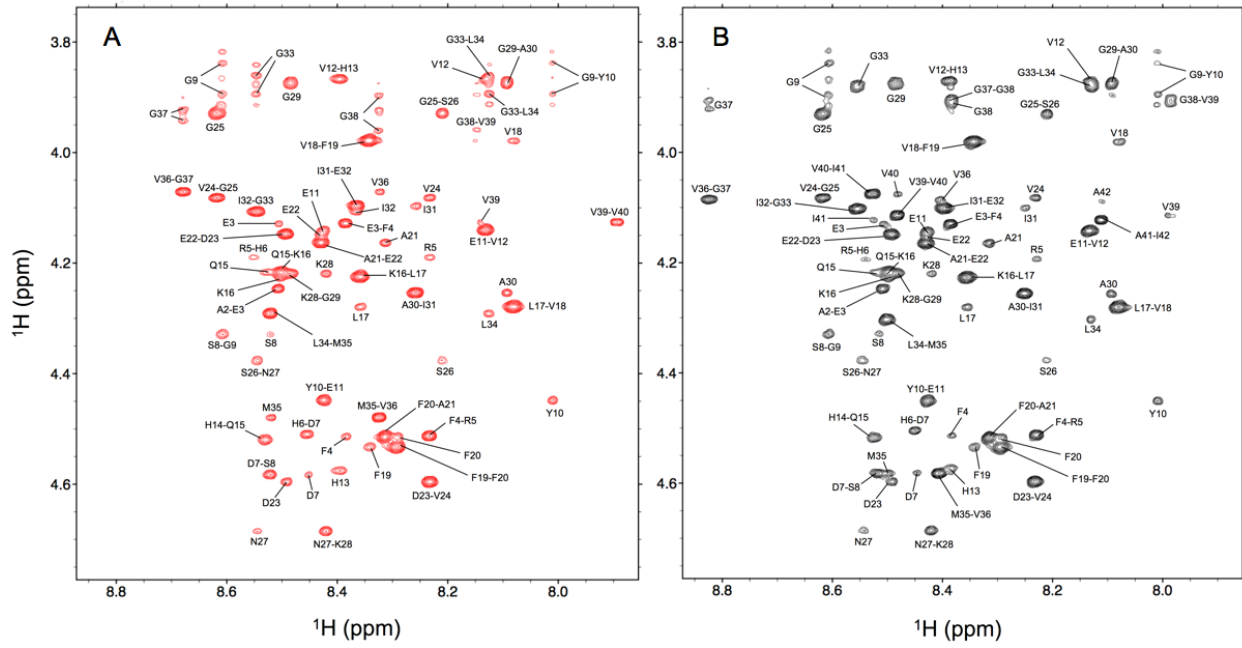


**Figure S3.** Expanded region of the 2D  $F_1$  BASH-decoupled NOESY spectrum recorded at 900 MHz for (A)  $\text{A}\beta^{1-40}$  and (B)  $\text{A}\beta^{1-42}$  at 277 K. The cross-peaks correspond to sequential and intraresidue couplings between the  ${}^1\text{H}^N$  and  ${}^1\text{H}^\alpha$  protons.

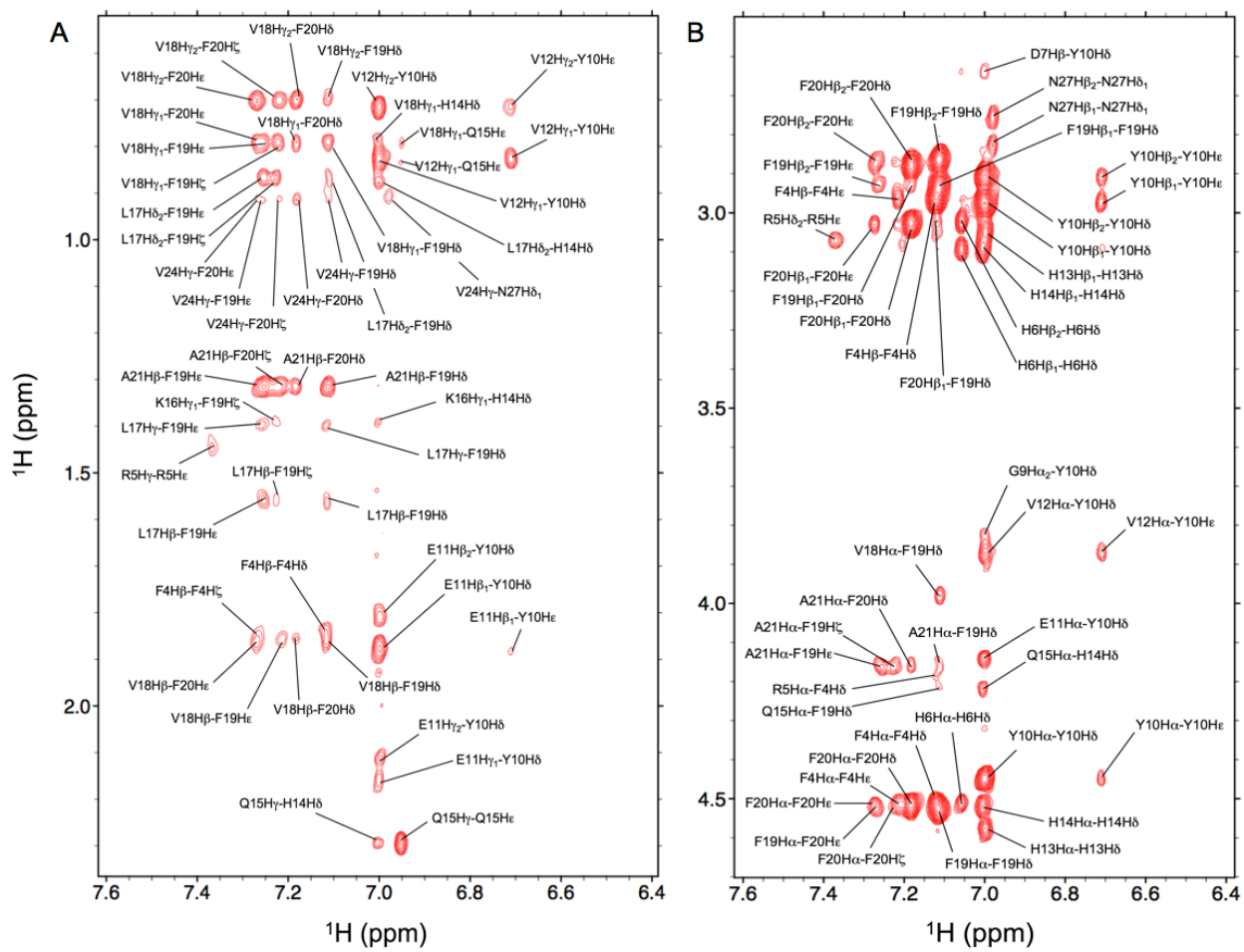


**Figure S4.** Expanded region of the 2D NOESY spectrum recorded at 900 MHz for the A $\beta$ <sup>1-40</sup> at 277 K. The aromatic region is shown with the corresponding assignment of the  $^1\text{H}$ - $^1\text{H}$  NOE contacts in (A) the aliphatic region and (B) the  $^1\text{H}^\alpha$  and  $^1\text{H}^\beta$  region.

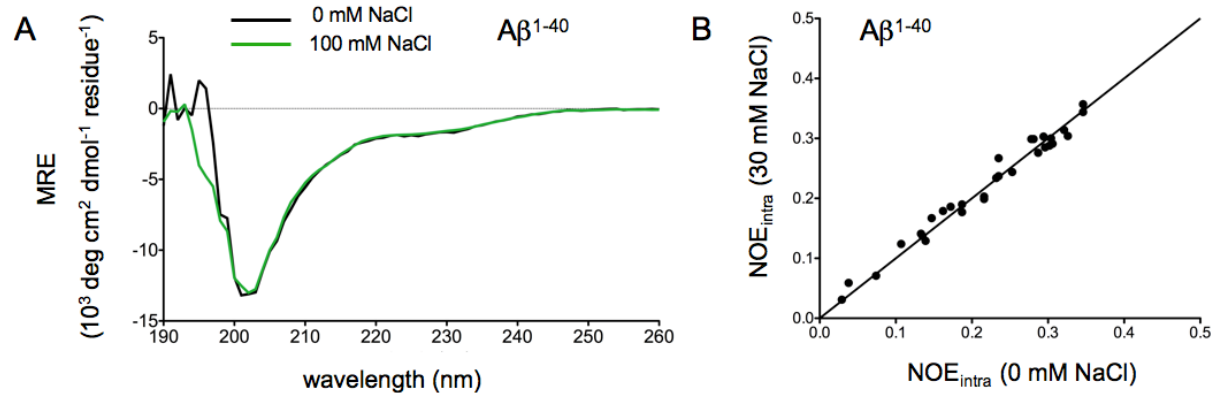


**Figure S5:** (A) Comparison of the CD spectra recorded at 288 K in 20 mM sodium phosphate pH 7.0, for 50  $\mu\text{M}$  samples of  $\text{A}\beta^{1-40}$  in the absence of NaCl (black) and in the presence of 100 mM NaCl (green). The CD spectra are recorded as the mean residue ellipticity (MRE). (B) Correlation between the intra-residue  $d_{\text{aN(i.i)}}$  NOE cross peak intensities extracted from 3D NOESY-HSQC spectra recorded at 277 K in 20 mM sodium phosphate pH 7.0 for 150  $\mu\text{M}$  samples of  $\text{A}\beta^{1-40}$  in the absence of NaCl and in the presence of 30 mM NaCl.

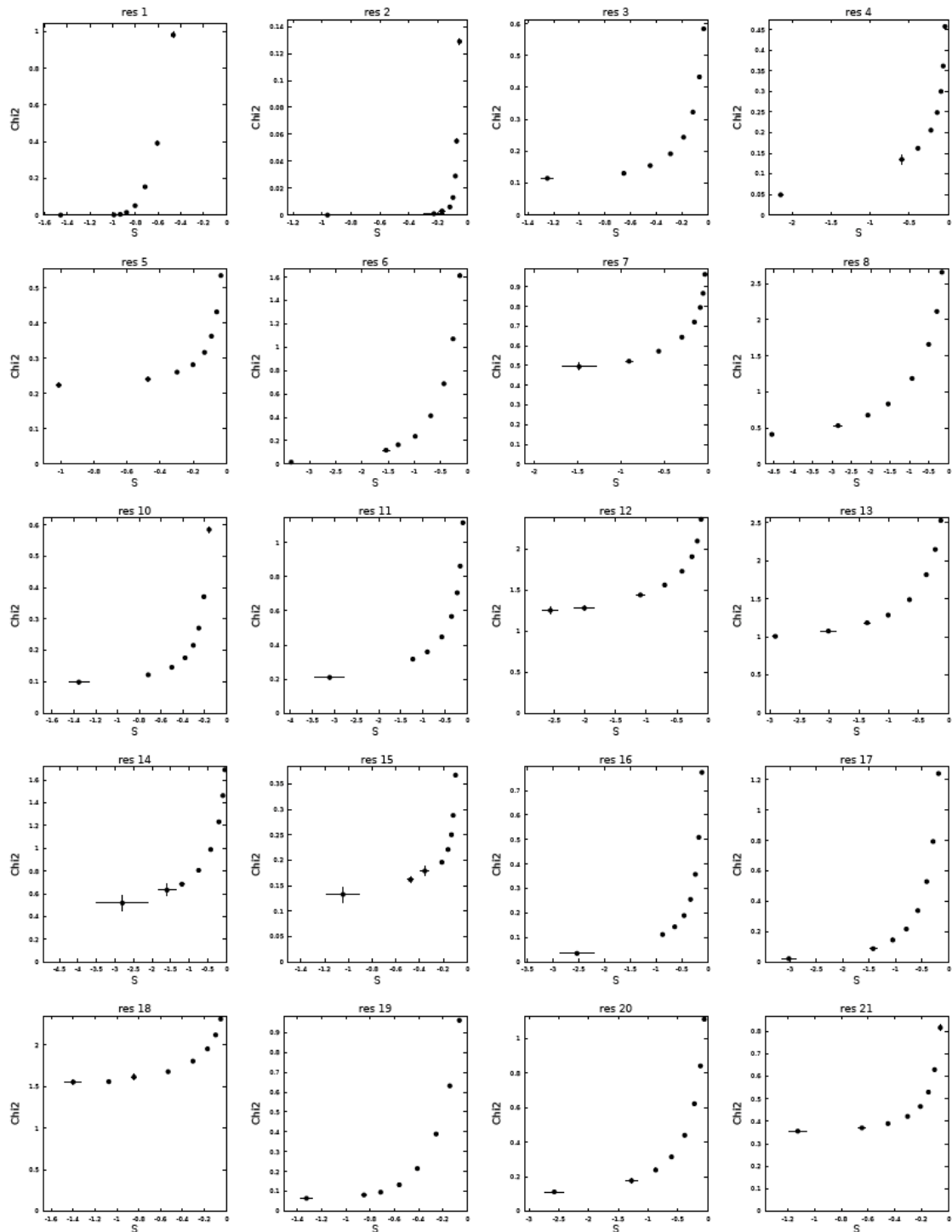


**Figure S6:** Plots of  $\chi^2$  versus  $S$ , the maximum entropy term, derived for different values of  $\theta$ , which controls the weight of the entropy term relative to that of the experimental data.<sup>6</sup> A set of  $\theta$ -values of (left to right) of 0, 0.1, 0.2, 0.4, 0.8, 1.6, 3.0, 6.0 and 10 was used here.

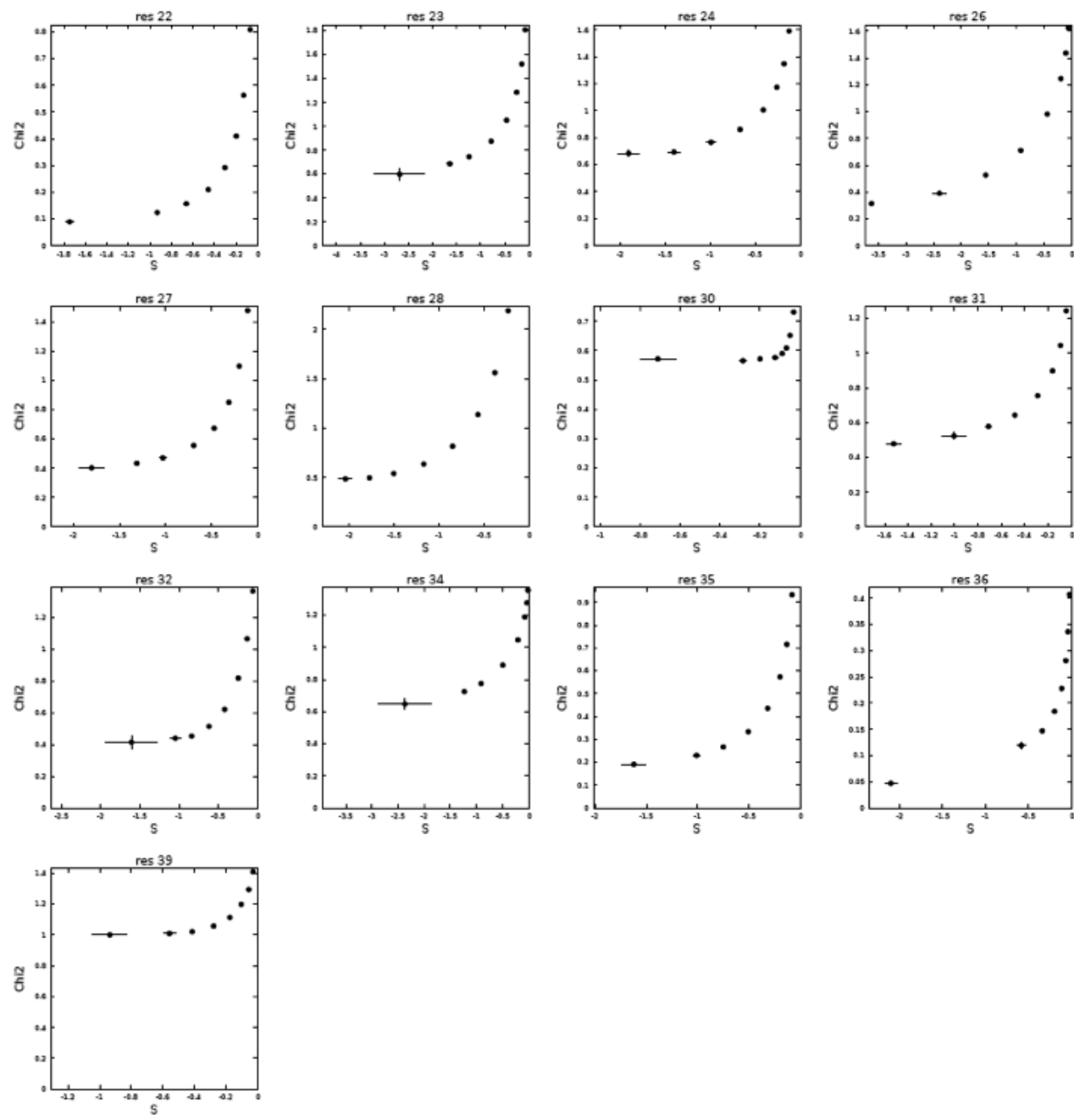


**Figure S6 (continued)**

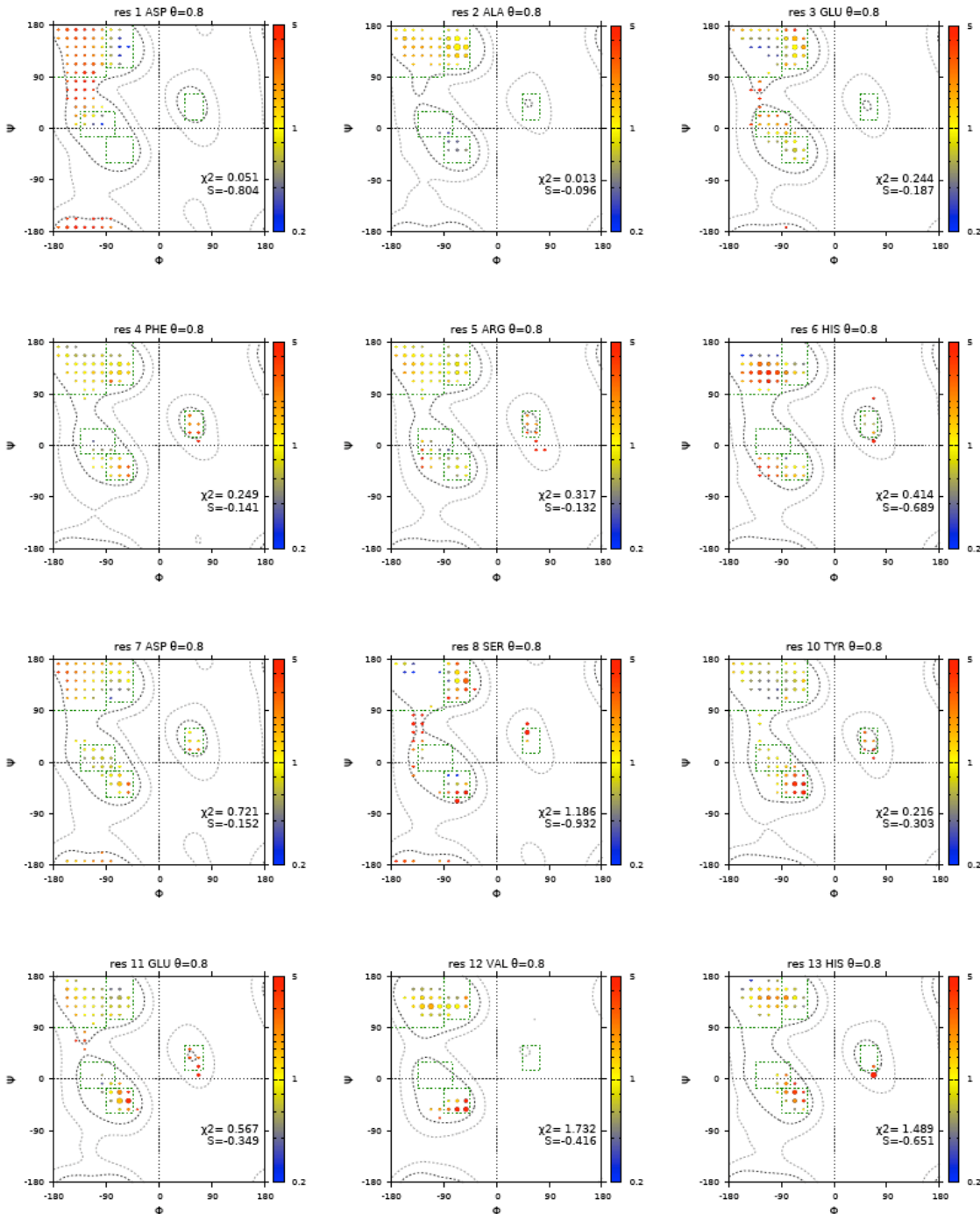


**Figure S7 (part1):**  $\phi/\psi$  torsion angle distributions derived for  $A\beta^{1-40}$  residues using the MERA webserver program.<sup>6</sup> The surface area of each circle is proportional to the population of its  $15^\circ \times 15^\circ$  voxel and the color of each circle reflects its fractional deviation from that seen in the coil database. Green boxes mark secondary structure regions:  $\beta$ , PPII,  $\alpha_L$ , type I  $\beta$ -turn ( $\beta$ -I) and  $\alpha_R$  (see Fig. 5, main text). An entropy weight factor of 0.8 and a diffusion anisotropy parameter  $k = 0.3$  were used. Heavy black dashed lines mark the edges of the most populated region of the residue-specific coil library and thin dashed lines mark the edges of sparsely populated regions.

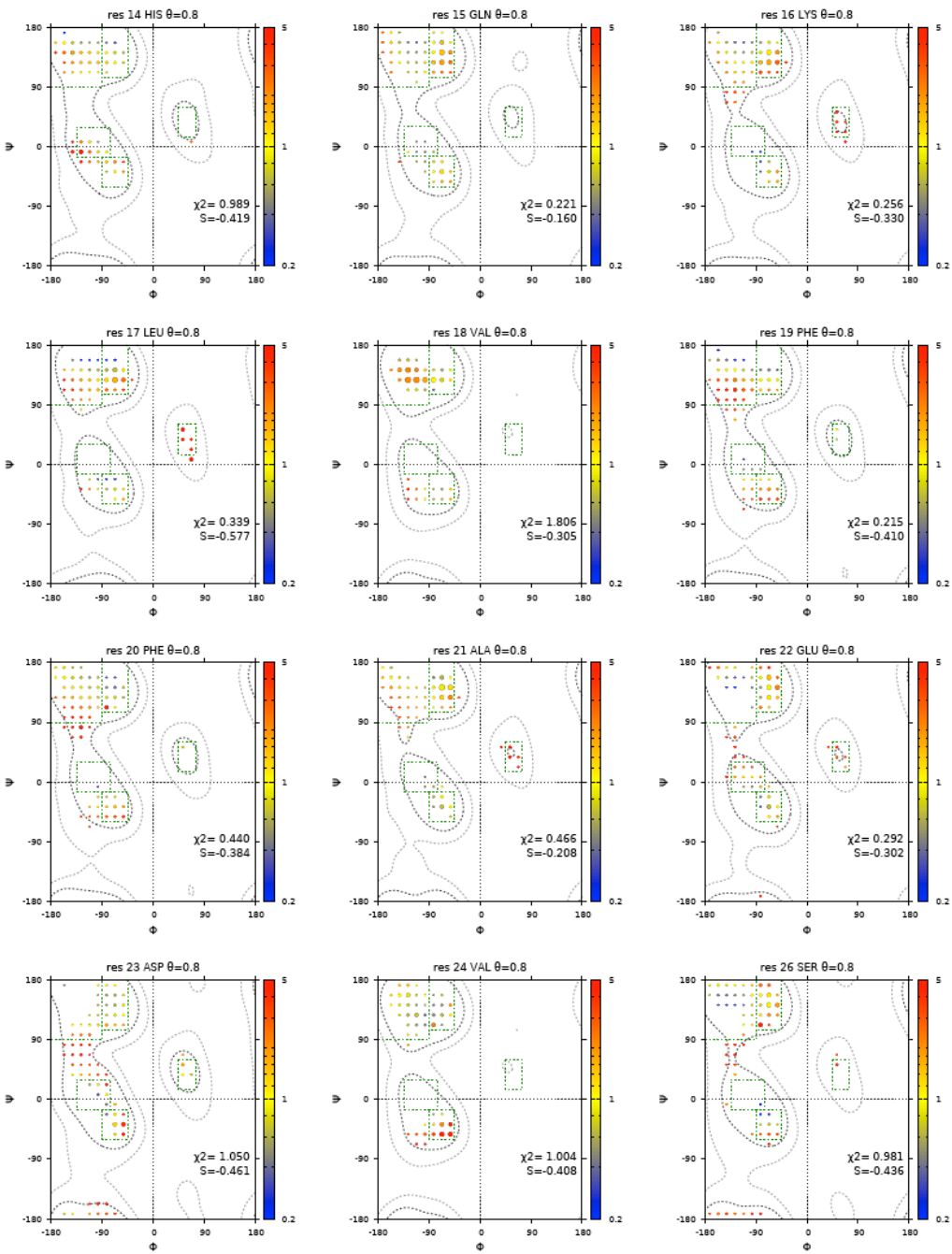


**Figure S7 (continued).**

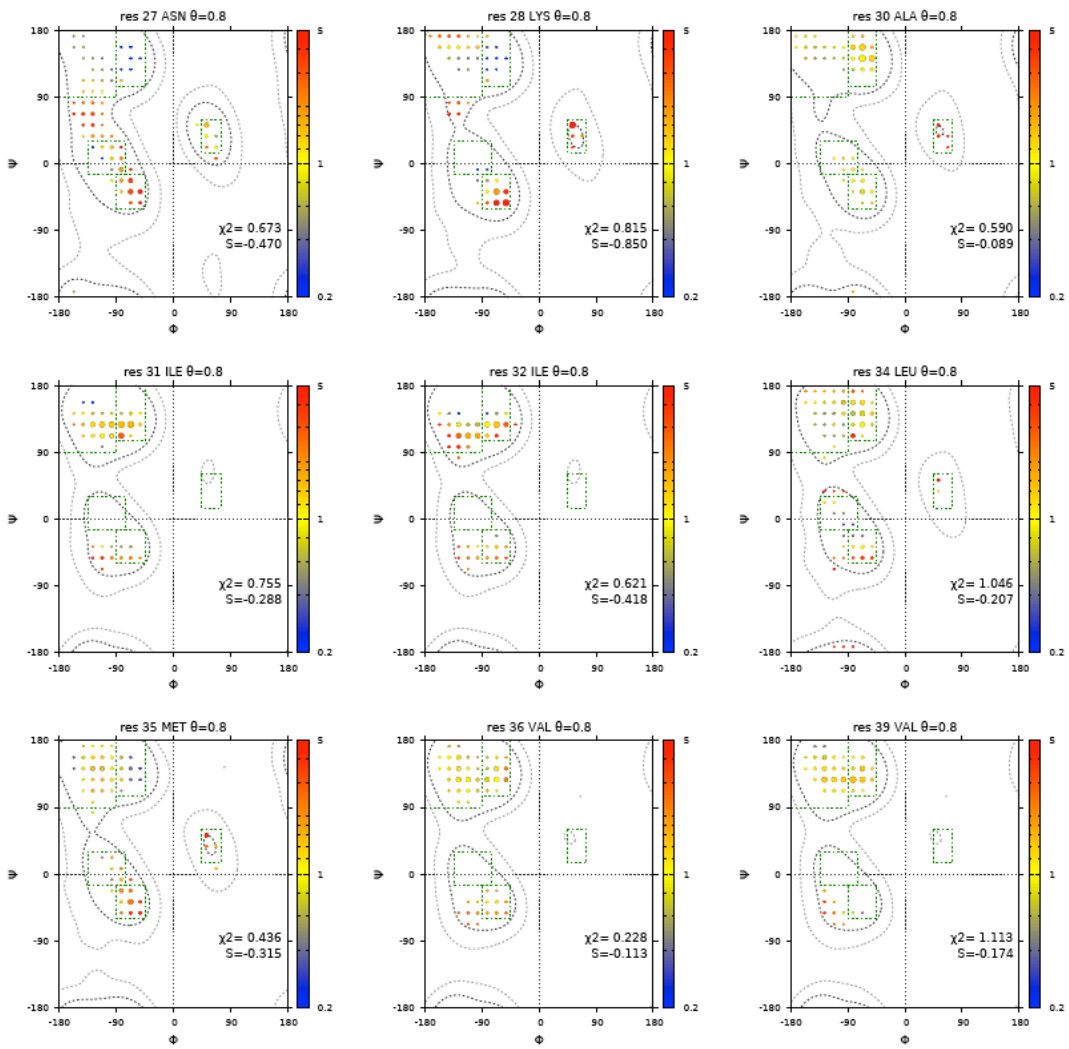


**Figure S7 (continued).**

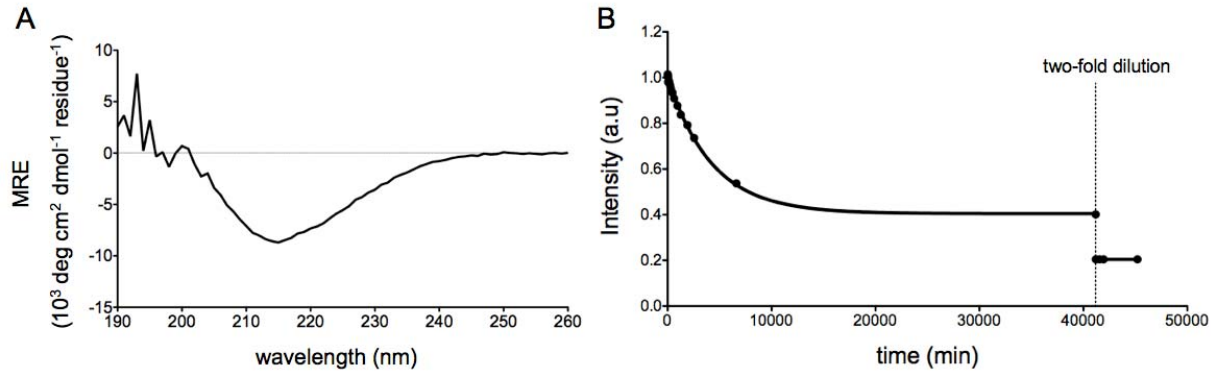


**Figure S8:** (A) CD spectrum recorded at 288 K for a 150  $\mu\text{M}$  sample of  $\text{A}\beta^{1-42}$  in 20 mM sodium phosphate pH 7.0 ( $\text{H}_2\text{O}$  sample) after 28 days at 4°C (see Fig. 6 in the main text and panel B). (B) The same sample was also used to monitor the evolution of methyl group cross peak intensities of in a series of 2D  $^1\text{H}/^{13}\text{C}$  after a two-fold dilution (from 150  $\mu\text{M}$  to 75  $\mu\text{M}$ ). Inspection of the diluted sample after 1 month of further storage at 4°C showed vanishingly weak intensities, i.e., nearly full aggregation of the sample.

## References

- Yamaguchi, T.; Matsuzaki, K.; Hoshino, M., *FEBS Lett.* **2011**, 585, 1097-1102.
- Waelti, M. A.; Orts, J.; Voegeli, B.; Campioni, S.; Riek, R., *ChemBioChem* **2015**, 16, 659-669.
- Kjaergaard, M.; Brander, S.; Poulsen, F. M., *J. Biomol. NMR* **2011**, 49, 139-149.
- Kjaergaard, M.; Poulsen, F. M., *J. Biomol. NMR* **2011**, 50, 157-165.
- Sgourakis, N. G.; Yan, Y.; McCallum, S. A.; Wang, C.; Garcia, A. E., *J. Mol. Biol.* **2007**, 368, 1448-1457.
- Mantsyzov, A. B.; Shen, Y.; Lee, J. H.; Hummer, G.; Bax, A., *J. Biomol. NMR* **2015**, 63, 85-95.

**Table S1:**  $^3J_{\text{H}\text{N}\text{H}\alpha}$  values measured for  $\text{A}\beta^{1-40}$  and  $\text{A}\beta^{1-42}$ 

	$\text{A}\beta^{1-40}$	$\text{A}\beta^{1-42}$
E3	$6.30 \pm 0.03$	$6.23 \pm 0.03$
F4	$7.02 \pm 0.05$	$7.02 \pm 0.05$
R5	$7.25 \pm 0.06$	$7.29 \pm 0.06$
D7	$6.86 \pm 0.12$	$6.89 \pm 0.13$
S8	$5.86 \pm 0.13$	$6.01 \pm 0.14$
G9	$6.35 \pm 0.19^{\text{a}}$	$6.27 \pm 0.20^{\text{a}}$
Y10	$6.38 \pm 0.07$	$6.39 \pm 0.07$
E11	$6.29 \pm 0.12$	$6.27 \pm 0.13$
V12	$6.78 \pm 0.12$	$6.77 \pm 0.12$
H13	$7.25 \pm 0.19$	$7.14 \pm 0.20$
Q15	$6.26 \pm 0.19$	$6.18 \pm 0.19$
K16	$6.22 \pm 0.18$	$6.30 \pm 0.18$
L17	$6.69 \pm 0.14$	$6.63 \pm 0.15$
V18	$8.30 \pm 0.11$	$8.20 \pm 0.12$
F19	$7.70 \pm 0.10$	$7.72 \pm 0.10$
F20	$7.74 \pm 0.10$	$7.67 \pm 0.11$
A21	$5.60 \pm 0.09$	$5.56 \pm 0.10$
E22	$5.95 \pm 0.06$	$5.86 \pm 0.06$
D23	$6.64 \pm 0.07$	$6.63 \pm 0.08$
V24	$6.82 \pm 0.06$	$6.75 \pm 0.06$
G25	$5.96 \pm 0.11^{\text{a}}$	$5.85 \pm 0.12^{\text{a}}$
S26	$6.51 \pm 0.07$	$6.53 \pm 0.12$
N27	$7.32 \pm 0.14$	$7.19 \pm 0.15$
K28	$6.46 \pm 0.07$	$6.43 \pm 0.12$
G29	$6.03 \pm 0.11^{\text{a}}$	$5.89 \pm 0.11^{\text{a}}$
A30	$5.49 \pm 0.04$	$5.41 \pm 0.04$
I31	$7.65 \pm 0.05$	$7.68 \pm 0.05$
I32	$7.45 \pm 0.06$	$7.41 \pm 0.07$
G33	$5.96 \pm 0.12^{\text{a}}$	$5.95 \pm 0.12^{\text{a}}$
L34	$6.72 \pm 0.04$	$6.78 \pm 0.05$
M35	$7.25 \pm 0.04$	$7.54 \pm 0.05$
V36	$7.49 \pm 0.04$	$7.68 \pm 0.04$
G37	$5.98 \pm 0.07^{\text{a}}$	$5.72 \pm 0.07^{\text{a}}$
G38	$5.99 \pm 0.06^{\text{a}}$	$5.87 \pm 0.06^{\text{a}}$
V39	$7.94 \pm 0.02$	$7.90 \pm 0.02$
V40	$8.62 \pm 0.02$	$7.80 \pm 0.02$
I41		$8.33 \pm 0.01$
A42		$6.55 \pm 0.02$

<sup>a</sup> Values reported for Gly correspond to  $(^3J_{\text{H}\text{N}\text{H}\alpha 2} + ^3J_{\text{H}\text{N}\text{H}\alpha 3})/2$

**Table S2:** Experimental parameters measured for A $\beta$ <sup>1-40</sup> used as input for the MERA program, including three types of chemical shifts (<sup>15</sup>N, <sup>13</sup>C $\alpha$  and <sup>13</sup>C'), six types of J couplings (<sup>3</sup>J<sub>HN-H $\alpha$</sub> , <sup>3</sup>J<sub>C'-C'</sub>, <sup>3</sup>J<sub>C'-H $\alpha$</sub> , <sup>1</sup>J<sub>H $\alpha$ -Ca</sub>, <sup>2</sup>J<sub>Ca-N</sub> and <sup>1</sup>J<sub>Ca-N</sub>) and three types of NOE (d<sub>NN</sub>(i,i+1); d<sub>aN</sub>(i,i); d<sub>aN</sub>(i,i+1)).

	<sup>13</sup> C $\alpha$	<sup>13</sup> C'	<sup>13</sup> N	<sup>3</sup> J <sub>HNH<math>\alpha</math></sub> $\pm 0.08$	<sup>1</sup> J <sub>H<math>\alpha</math>Ca</sub> $\pm 0.06$	<sup>2</sup> J <sub>CaN</sub> $\pm 0.11$	<sup>1</sup> J <sub>NC<math>\alpha</math></sub> $\pm 0.11$	<sup>3</sup> J <sub>C'C'</sub> $\pm 0.09$	<sup>3</sup> J <sub>C'H<math>\alpha</math></sub> $\pm 0.10$	d <sub>aN</sub> (i,i) $\pm 0.011$	d <sub>aN</sub> (i,i+1) $\pm 0.003$	d <sub>NN</sub> (i,i+1) $\pm 0.001$	J(0)*10 <sup>-10</sup>
D1	53.270	-	-	-	-	-	-	-	-	-	-	-	-
A2	52.248	177.326	-	-	144.01	-	-	-	-	-	-	-	-
E3	56.433	176.074	120.760	6.30	142.14	8.04	10.79	0.77	1.99	0.074	0.427	0.077	3.628
F4	57.467	175.298	122.040	7.02	145.14	7.95	10.78	1.01	2.62	0.133	0.704	0.096	4.721
R5	55.468	175.619	123.790	7.25	142.51	7.95	10.85	1.16	2.63	0.187	0.690	0.237	5.546
H6	55.787	174.778	121.310	-	144.18	8.26	10.49	1.10	2.87	-	-	-	6.679
D7	53.933	176.339	121.920	6.86	143.45	7.75	10.94	1.04	2.45	0.216	0.562	0.189	7.058
S8	58.978	175.220	116.870	5.86	142.20	7.97	10.89	1.01	2.28	0.216	0.557	0.225	7.405
G9	45.173	174.057	110.980	6.35	141.07	7.06	11.18	0.93	-	-	-	0.283	7.036
Y10	58.259	175.831	120.360	6.38	144.27	7.59	10.68	0.93	2.34	0.253	0.732	0.238	8.748
E11	56.414	176.178	122.730	6.29	143.16	7.32	10.57	0.90	2.44	0.294	0.939	0.175	9.626
V12	62.689	176.055	121.480	6.78	143.37	7.98	10.28	0.91	2.49	0.321	1.325	0.148	9.634
H13	55.647	174.959	122.330	7.25	143.98	7.24	11.09	0.81	2.78	0.346	1.325	0.148	9.634
H14	55.882	174.925	120.990	-	143.79	7.40	10.84	-	-	-	-	-	9.634
Q15	55.730	175.703	121.840	6.26	143.35	8.26	10.73	0.89	1.83	0.346	1.287	0.305	9.634
K16	56.214	176.249	123.600	6.22	142.63	8.10	10.50	0.87	2.41	0.302	1.348	0.157	10.106
L17	54.948	176.784	124.340	6.69	142.37	8.05	10.25	0.84	2.85	0.326	1.349	0.253	9.676
V18	61.763	175.143	121.840	8.30	142.66	8.00	10.63	1.16	2.82	0.304	1.593	0.235	9.676
F19	57.278	174.795	124.710	7.70	143.89	8.05	10.35	1.23	2.46	0.287	1.449	0.214	9.403
F20	57.131	174.745	123.300	7.74	143.41	8.20	10.50	1.36	-	0.281	1.061	0.186	8.953
A21	52.192	177.276	126.430	5.60	143.91	8.05	10.85	0.94	2.20	0.296	0.983	0.144	8.281
E22	56.425	176.157	120.220	5.95	141.99	8.11	10.66	0.80	2.12	0.187	0.816	0.178	8.014
D23	53.905	176.625	122.060	6.64	142.65	7.82	10.43	0.90	2.37	0.278	0.640	0.135	7.702
V24	62.656	177.116	120.960	6.82	142.62	7.81	10.26	0.96	2.35	0.232	0.647	0.194	7.012
G25	45.277	174.538	111.970	5.96	140.81	7.12	11.24	0.76	3.94	-	-	0.142	7.181
S26	58.383	174.523	115.710	6.51	142.39	8.22	11.25	0.95	2.16	0.235	0.684	0.183	6.711
N27	53.109	175.504	120.760	7.32	142.33	7.04	10.19	1.01	2.91	0.235	0.564	0.179	5.697
K28	56.560	177.232	121.970	6.46	142.63	7.71	10.25	0.95	2.67	0.306	0.466	0.190	6.178
G29	44.934	173.744	109.760	6.03	140.61	7.46	11.51	0.74	3.86	-	-	0.160	5.531
A30	52.385	177.673	123.750	5.49	143.82	8.15	11.05	0.71	2.04	0.147	0.657	0.099	6.261
I31	60.896	176.472	121.030	7.65	142.65	8.23	10.27	0.86	2.28	0.172	0.635	0.113	5.797
I32	61.026	176.682	126.600	7.45	142.15	7.70	10.10	0.96	-	0.139	0.840	0.106	6.254
G33	44.928	173.720	113.360	5.96	139.78	7.99	11.47	0.78	-	-	-	0.117	6.102
L34	54.945	177.356	121.870	6.72	142.26	8.49	10.51	0.72	2.21	0.135	0.498	0.085	5.567
M35	55.076	176.195	122.260	7.25	142.54	7.88	10.65	0.88	2.51	0.162	0.406	0.071	4.973
V36	62.421	176.738	122.730	7.49	142.02	7.99	10.64	1.06	2.42	0.107	0.508	0.075	3.794
G37	44.993	174.494	113.430	5.98	140.57	7.99	11.48	0.81	-	-	-	0.083	3.808
G38	44.830	173.723	108.890	5.99	140.42	8.55	11.97	0.84	-	-	-	0.034	2.701
V39	62.323	175.602	120.130	7.94	141.82	8.68	10.67	0.99	2.36	0.038	0.172	0.025	2.225
V40	63.667	-	128.630	8.62	141.75	7.45	9.75	-	2.61	0.029	-	-	1.656